TU Delft

Delft University of Technology

The influence of CO_2 on NO reduction into N_2 over reduced ceria-based catalyst

Wang, Yixiao; Makkee, Michiel

DOI
10.1016/j.apcatb.2017.09.013

Publication date
2018

Document Version
Accepted author manuscript

Published in
Applied Catalysis B: Environmental

Citation (APA)
Wang, Y., & Makkee, M. (2018). The influence of CO_2 on NO reduction into N_2 over reduced ceria-based catalyst. *Applied Catalysis B: Environmental*, *221*, 196-205. https://doi.org/10.1016/j.apcatb.2017.09.013

Important note
To cite this publication, please use the final published version (if applicable).
Please check the document version above.

Copyright
Other than for strictly personal use, it is not permitted to download, forward or distribute the text or part of it, without the consent of the author(s) and/or copyright holder(s), unless the work is under an open content license such as Creative Commons.

Takedown policy
Please contact us and provide details if you believe this document breaches copyrights.
We will remove access to the work immediately and investigate your claim.

This work is downloaded from Delft University of Technology.
For technical reasons the number of authors shown on this cover page is limited to a maximum of 10.

© 2017 Manuscript version made available under CC-BY-NC-ND 4.0 license https://creativecommons.org/licenses/by-nc-nd/4.0/
Link to formal publication Applied Catalysis B: Environmental (Elsevier): https://doi.org/10.1016/j.apcatb.2017.09.013

The influence of CO_2 on NO reduction into N_2 over reduced ceria-based catalyst

Yixiao Wang and Michiel Makkee*

Catalysis Engineering, Chemical Engineering Department, Faculty of Applied Sciences Delft University of Technology, Van der Maasweg 9 ,2629 HZ Delft, The Netherlands

E-mail: m.makkee@tudelft.nl

Abstract

Oxygen defects in reduced ceria are the catalytic sites for the NO reduction into N_2 in the Toyota Di-Air $DeNO_x$ abatement technology. Traces of NO (several hundred ppm) have to compete with the excess amount of other oxidants, *e.g.,* 5% CO_2 and 5% O_2, in an exhaust gas of a lean burn (diesel) engine. The reactivities of CO_2 and NO over a reduced ceria and noble metal loaded reduced ceria have been investigated under ultra-high vacuum system in TAP and under atmosphere pressure in *in-situ* Raman and flow reactor set-up. The results showed that CO_2 was a mild oxidant which was able to oxidise the oxygen defects, but hardly oxidised deposited carbon over both ceria and noble metal loaded ceria. NO was a stronger oxidant and more efficient in refilling the oxygen defects and able to convert the deposited carbon, which acted as buffer reductant to extend the NO reduction time interval. NO was selectively and completely converted into N_2. The presence of excess CO_2 hardly affected the NO reduction process into N_2.

Keywords: Ceria, noble metal, oxygen defects, CO_2 activation, NO reduction

1. Introduction

For diesel powered vehicles, due to the more stringent NO_x emission standard and emission test certifications, more effective and advanced exhaust emission after-treatment technologies are required. The by EU commission in 2017 introduced realistic driving emission (RDE) forces significantly to improve the current $DeNO_x$ technologies, *i.e.,* NO_x Storage and Reduction (NSR) [1], Selective Catalytic Reduction (SCR) [2], and the combination thereof [3]. Recently, Bisaiji *et al*. (Toyota Company) developed a new emission control technology, the Di-Air system (Diesel $deNO_x$ System by Adsorbed Intermediate Reductants). In this system, short rich and lean periods are created by high frequency direct diesel fuel injection downstream of the engine into the exhaust upstream of a NSR catalyst (an unspecified complex mixture of $Pt/Rh/Ba/K/Ce/Al_2O_3$ coated onto a monolith) [4, 5]. These pulses will reduce the catalyst and create carbon deposits on the catalyst [6]. The Di-Air system promises to meet future emission standards under realistic driving test conditions. Oxygen defects in a reduced ceria have been identified to be the catalytic sites for the selective conversion of NO into N_2 [6]. Deposited carbon on the reduced ceria created during diesel fuel injection acts as a buffer reductant. The oxidation of deposited carbon via the ceria lattice oxygen species will recreate new oxygen defects in the ceria lattice. These recreated ceria oxygen defects provide an additional NO conversion capacity [6].

In the exhaust gas of a lean burn engine, the concentration of O_2 and CO_2 (around 5%) are much higher than that of NO (in the order of a few hundred ppm). In a previous article we have demonstrated that even in the excess of oxygen NO is completely converted into N_2 (100 % NO conversion with 30 % efficiency with respect to oxygen at an O_2 to NO ratio of 100) at 450 °C for bare ceria and noble metal loaded ceria [7]. CO_2 will also be capable to oxidise these oxygen defect sites of reduced ceria [8], which has been commonly reported in the field of solar fuel cells [9]. Metal and/or metal oxide interaction or boundary regions are claimed to further assist in the CO_2 dissociation over the noble metal loaded ceria [10, 11]. Although the universal mechanism of CO_2 activation into CO and (atomic or molecular) oxygen is still unresolved [12, 13], the CO_2 activation via dissociation was extensively reported both by DFT modelling study and some experimental work. To best of our knowledge, no work has been published on the efficiency and reactivity of CO_2 *versus* the number of oxygen defects in ceria. Especially, the relative reactivity of CO_2 *versus* NO will be crucial for the Di-Air system optimisation. The oxidation of deposited carbon by CO_2 should be minimised in order to

maximise the function of deposited carbon as a buffer reductant for the NO reduction. Furthermore, the study of NO reactivity and selectivity in the presence of CO_2 are essential, as the commonly reported side products especially over noble metal catalysts, *e.g.,* N_2O and NO_2, have an even worse effect on our environment and human health.

Therefore, Temporal Analysis of Products (TAP, ultra-high vacuum) technique was applied to study the reactivity of CO_2 and NO *versus* the number of oxygen defects and deposited carbon over ceria and noble metal loaded ceria. *In-situ* Raman (atmosphere pressure) and fixed bed flow reactor experiments were performed to confirm the TAP results. More importantly, the competition of small amount of NO with an excess of CO_2 was performed in a fixed-bed flow reactor in order to mimic the selectivity and reactivity of NO reduction under more realistic conditions.

Commercially available Zr and La-doped ceria (a gift of BASF, further denoted as ceria) was used as a model of ceria due to its high hydrothermal stability [6, 14, 15]. The concept of the hypothetical ceria layer was introduced to describe the oxidation state of the ceria. Each O-Ce-O tri-layer is regarded as one hypothetical ceria layer. The number of reducible oxygen defects on one hypothetical reduced ceria layer were calculated to be $2.6 \cdot 10^{17}$ oxygen atoms / mg_{cat} for an agglomerate of ceria with a mean average particle size of 5 nm [6, 16]. Based on these assumptions and calculations a cubical ceria particle of 5 nm will be built up from 16 O-Ce-O tri-layers.

2. Materials and methods

2.1. Materials preparation

0.5 wt % Rh/ceria and Pd/ceria were prepared via an incipient wetness impregnation method on dried ceria. Rhodium(III) nitrate hydrate and Palladium(II) nitrate hydrate (purchased from Sigma Aldrich) were used as the precursors in purified demi water. Subsequently, the samples were dried at 110 $^{\circ}C$ overnight and calcined at 550 $^{\circ}C$ for 5 h.

2.2. Characterisation

2.2.1. Inductively Coupled Plasma Optical Emission Spectroscopy (ICP-OES)

Approximately 50 mg of catalyst was destructed in 4.5 mL 30% HCl + 1.5 mL 65% HNO_3 in a microwave for 120 min. at max. power of 900 W. After destruction the samples were diluted to 50 mL

with Millipore-Q (purified demi) water. The samples were analysed with ICP-OES (PerkinElmer Optima 5300).

2.2.2. N_2 adsorption

Tristar II 3020 Micromeritics was used to determine the textural properties like specific BET surface area and pore volume at -196 °C. The catalyst samples were degassed at 200 °C for 16 h in vacuum (0.05 mbar) prior to the nitrogen adsorption.

2.2.3. X-ray diffraction (XRD)

The Powder X-Ray diffraction (XRD) was recorded on a Bruker-AXS D5005 with a Co *Kα* source. The data were 3 times collected by varying the 2θ angle from 5° to 90° with a step size of 0.02.

2.2.4. H_2-TPR

TPR (temperature programmed reaction with hydrogen) for the ceria, Rh/ceria, and Pd/ceria were carried out in home-made fixed bed reactor system connected to a thermal conductivity detector (TCD) to monitor the consumption of hydrogen by the (catalyst) sample. 200 mg of sample was packed between SiC layers (particle sizes: 300-425 µm). The sample was then reacted with H_2 (10%)/Ar flow with a flow rate of 30 ml_{STP} min^{-1} at a constant heating rate of 5 °C/min from room temperature to 1000 °C. TCD was calibrated by using CuO as a reference. A perma pure tubular drier was used to remove the water produced during the reaction upstream of the TCD detector.

2.3. Catalytic testing

2.3.1. TAP experiments under ultra-high vacuum condition

The pulse experiments were carried out in an in-house developed TAP (Temporal Analysis of Products) reactor. Small gas pulses, typically in the order of $1 \cdot 10^{15}$ molecules, were introduced in a small volume (1 mL) upstream of the catalyst fixed bed reactor. The produced pressure gradient over the catalyst packed bed, thereby, caused the molecules to be transported through the packed bed to the ultra-low vacuum at the opposite side of the reactor bed. Depending on the actual amount of molecules pulsed, the transport can be purely Knudsen diffusion. In other words, the molecules will only interact with the 'walls' (catalyst surface and reactor walls) of the system and not with each other. Upon interaction with the catalyst, the molecules can be converted into different products. The

evolution of the reactant and product molecules are tracked (one mass at a time) in time by means of a mass spectrometer with a high resolution of 10 kHz. More details about TAP can be found in elsewhere [6].

21.2 mg of ceria, 10 mg of Rh/ ceria, and 10 mg of Pd/ceria (100-250 μm) were used and loaded as a fixed bed reactor in the TAP equipment. For all measurements, the gas pulses contained either 20 vol. % Ne or 20 vol. % Ar or 20 vol. % Kr as an internal standard. In all experiments, the catalyst was initially oxidised by admitting O_2/Ar pulses until the O_2 signal approached a stable level. Reductions of ceria or noble metal loaded ceria were subsequently performed using reductant pulses of either 80 vol. % C_3H_6 in Ne or 80 vol. % CO in Ar. The re-oxidation was conducted using oxidant pulses of either 80 vol. % CO_2 or 80 vol. % NO both in Ar or 80 vol. % ^{15}NO in Kr. In all experiments a starting pulse size of approximately $1.6.10^{15}$ molecules was used, the pulse size gradually decreases during an experiment since the reactant was injected from a closed volume of a pulse-valve line.

The oxygen and carbon mass balances during the CO_2 or NO pulsing over the CO and C_3H_6 pre-reduced catalyst were calculated by Equation 1 and 2, respectively.

$$O_{balance} = (2 \times CO_{2\,in})/(or\ NO_{in}) - 2 \times CO_{2\,out} - CO_{out} - NO_{out} \quad [1]$$

$$C_{balance} = CO_{2\,in} - CO_{2\,out} - CO_{out} \quad [2]$$

A positive of $O_{balance}$ meant that oxygen accumulated in/on the catalyst, while a negative $C_{balance}$ indicated the consumption of deposited carbon from the catalyst.

2.3.2. *In-situ* Raman in Linkam cell

In-situ Raman spectra (Renishaw, 2000) were recorded using a temperature controlled *in-situ* Raman cell (Linkam, THMS 600). Ten scans were collected for each spectrum in the 100-4000 cm^{-1} range using continuous grating mode with a resolution of 4 cm^{-1} and scan time of 10 s. The excitation wavelength was 325 nm. The power of each laser line was kept at about 2.5 mW to prevent local heating effects. The spectrometer was daily calibrated using a silicon standard with a strong absorption band at 520 cm^{-1}. The (re-oxidised) ceria was pre-treated by C_3H_6 (1000 ppm in N_2, flow rate 200 mL/min) for 2 h. N_2 was used to flush the cell for 20 min. Subsequently, either 1000 ppm CO_2 or 1000 ppm NO both in N_2 with a flow rate of 200 mL/min was admitted to the cell.

2.3.3. Flow reactor experiment under atmosphere pressure

The catalyst sample (200 mg) was placed in a 6 mm inner diameter quartz reactor tube and equipped downstream with a mass spectrometry (MS, Hiden Analytical, HPR-20 QIC) and an infrared (IR) spectroscopy (Perkin–Elmer, Spectrum One). For the IR analysis a gas cell with KBr windows with an internal path length of ~5 cm was used. The spectra were recorded in a continuous mode using the Perkin-Elmer 'Time-Base' software between 4000 - 700 cm^{-1} wavenumbers with a spectral resolution of 8 cm^{-1} and an acquisition of 8 scans per spectrum, resulting in a time interval of 23 s between each displayed spectrum.

The Raman spectroscopy measurements were performed under reaction conditions by using an AvaRaman-PRB-FC Raman probe. Raman data were collected using a Kaiser Optical Systems RXN spectrometer with a diode laser operating at 532 nm and output power of 10 mW. Raman probe was used to focus the laser beam to a spot and to collect the scattered radiation behaviour. A CCD camera was used to record the data using the Thermo Galactic Grams AI v. 7.0 software. Spectra were acquired using 2 scans at a resolution of 0.3 cm^{-1} in the range between 100 (detector cut-off) and 4350 cm^{-1}.

In all experiments, the catalyst was initially (re-)oxidised by O_2/He until the O_2 signal reached a stable level in MS. Reduction of catalyst was performed by flowing 1.25% C_3H_6 in He for 2 h with a flow rate of 200 ml/min and subsequently flushed with He (200 mL/min) for 30 min at 450 °C or 500 °C. Feed compositions of either 0.2% NO/He or 0.2% CO_2/He or (0.2% NO + 5% CO_2)/He were used at a GHSV of 67.000 L/L/h in the catalyst reduction experiments.

3. Results and discussion

3.1. Characterisation

3.1.1. Structure and chemical composition

Figure 1 (here)

Characterisation details of the ceria support were reported in more detail elsewhere [6, 16]. In brief, typical fluorite structure of ceria was detected by Raman and XRD. A 5 nm crystal size of ceria was

determined by the Scherrer's equation and confirmed by the analysis of the TEM micrographs. The bulk composition of ceria support was measured by ICP, which showed that the atomic ratio of Ce, Zr, and La was 0.64 : 0.15 : 0.21. The BET surface area of bare (fresh and spent) ceria was 65 m^2/g. The BET surface areas of Rh/ceria and Pd/ceria (fresh and spent) were similar to the bare ceria support (66 ± 2 m^2/g). The loadings of Rh and Pd were determined to be 0.5 wt %, measured by ICP-OES (0.0486 mmol/g_{cat} and 0.0470 mmol/g_{cat} of Rh and Pd loading, respectively). **Figure 1** showed the XRD patterns of ceria, Rh/ceria, and Pd/ceria. The patterns of both Rh/ceria and Pd/ ceria showed a fluorite cubic structure of ceria. Diffraction lines due to Rh and Pd metals or any rhodium and palladium oxides were not observed due to the low loading (0.5 wt %) and high dispersion of these noble metals on the ceria.

3.1.3. H_2-TPR

Figure 2 (here**)**

The reduction properties of bare ceria t and Rh- and Pd-loaded ceria were studied by H_2-TPR technique. The H_2-TPR results were presented in **Figure 2**. Ceria showed two peaks centred at 430 and 550 °C. It was generally accepted that the low temperature (430 °C) process was attributed to the surface reduction, whereas the high temperature (550 °C) was accounted for the bulk reduction [17]. The total H_2 consumption was calculated to be 1.2 mmol/g_{cat}, corresponding to 2.7 ceria layer reduction. The H_2 consumption up to temperatures of 500 °C (surface reduction) was calculated to be 0.4 mmol/g_{cat}, corresponding to around 0.9 ceria layers reduction.

For Pd/ceria, the peak area at 50 °C with a H_2 consumption of 0.05 mmol/g_{cat} was contributed from the reduction of PdO to Pd. The amount of H_2 consumption was almost equal to the Pd loading and in agreement with the literature [18]. The peak area centered at 350 °C was related to the surface reduction of ceria support with a H_2 consumption of 0.55 mmol/g_{cat}, corresponding to around 1.2 ceria layers reduction. The total H_2 consumption up to temperatures of 500 °C was calculated to be 1.3 mmol/g_{cat}, corresponding to 2.9 ceria layers reduction.

For Rh/ceria, the peak area with H_2 consumption of 0.3 mmol/g_{cat} centered at 100 °C which was larger than the amount needed for the reduction of Rh_2O_3 (or other type of RhO_x) to Rh (0.05 mmol/g_{cat} of Rh loading). Therefore, the hydrogen consumption was a combination reduction of Rh_2O_3 to Rh and a

partial reduction of CeO_2 into Ce_2O_3. The total H_2 reduction was calculated up to a temperature of 350 °C to be 1.7 mmol/ g_{cat}, corresponding to 3.8 layer ceria reduction.

3.2. Catalytic testing

3.2.1. Investigation of CO_2 and NO reactivity over reduced ceria support by TAP

To investigate the reactivity of CO_2 and NO towards the oxygen defects of ceria, CO and C_3H_6 were applied as reductants to pre-treat the catalyst samples. Table 1 summarises the result of CO and C_3H_6 pre-treatment over (re-oxidised) ceria [19].

Table 1. Summary of oxygen defects and deposited carbon by CO and C_3H_6 pre-treatment over ceria.

	T/ °C	Oxygen defects		Deposited carbon (carbon atoms/ mg_{cat})
		Oxygen atoms/ mg_{cat}	Ceria reduction layers	
CO	580	$3 \cdot 10^{17}$	1	-
	540	$3 \cdot 10^{17}$	1	-
C_3H_6	580	$7.1 \cdot 10^{17}$	2.8	$1.5 \cdot 10^{18}$
	560	$5.9 \cdot 10^{17}$	2.3	$1 \cdot 10^{18}$

Figure 3 (here)

The conversion of CO_2 over CO pre-reduced ceria at 580 °C was presented in **Figure 3A and B**. As shown in **Figure 3A** during the first several CO_2 pulses, the CO_2 conversion was almost 100%, accompanying with CO formation. Then the CO_2 conversion quickly declined until to nearly zero conversion after 14000 CO_2 pulses. CO_2 was able to produce oxygen species and to re-oxidise reduced ceria [20]. This made CO_2 a promising oxygen source or oxidant in partial oxidation reactions such as methane reforming [12] and oxidative dehydrogenation (ODH) of alkanes [21].. The carbon

balance during the CO_2 pulses (**Figure 3B**) showed a maximum 13% of carbon species was left on the ceria surface. Therefore, more than 85% of CO_2 was converted into CO with O filling the oxygen defects of ceria. The missing carbon species could due to the slow desorption of CO and CO_2 from the ceria surface. It might be argued that the missing carbon can form carbonate over the ceria. Tthe exposure of ceria with CO_2 can lead to the formation of carbonate over ceria [22, 23]. However, over a reduced ceria surface, the formation of carbonate can be largely limited. A DFT calculation result had shown that CO_2 was favoured to chemisorb to a reduced ceria resulting in the formation of an activated mono - dentate carbonate species, which can be further dissociated to form CO [24]. Regarding to the activation of CO_2 over a reduced ceria, the assistance with a hydroxyl group could be largely eliminated, since CO_2 pulses experiments were performed in a high vacuum system. Oxygen anion vacancies and the associated electrons should be regarding as the active sites to activate CO_2 [24]. Therefore, the pathway of CO_2 activation *via* surface hydroxyl group could be largely ruled out and had to proceed *via* a C=O bond activation. The charges had to be transferred from a reduced ceria to CO_2, resulting in the formation of CO_2^- anion radical species [25]. In general , the CO_2 activation over oxygen anion defect sites resulted in that one of CO_2's O atoms was used to fill the oxygen anion defect site and, thereby, re-oxidising the reduced ceria in combination with the desorption of one CO molecule (Equation 3):

$$CO_2 + 2Ce^{3+} \leftrightharpoons CO + 2Ce^{4+} + O^{2-} \quad (3)$$

Till 2000 pulses around half of the oxygen defects were filled. The experiments of CO_2 pulses over CO reduced ceria were also investigated at a lower temperature, *e.g.,* 300 ^{o}C. The experiments showed that CO_2 can be reduced to CO with O filling into oxygen defects. The effectiveness of CO_2 pulses was, however, lower, when the reaction temperature was lowered.

The NO pulses over the CO reduced ceria at 540 $^{\circ}$C showed that NO was completely converted into N_2 during the first 2000 NO pulses, followed by a breakthrough of NO (**Figure 3C**). Around 75% of the oxygen defects were refilled when the NO conversion started to drop (**Figure 3D**). N_2 was the exclusive product during the NO reduction. N_2O and NO_2 were not observed (detection limit of 1 ppm).

The different observations between CO_2 and NO pulses indicated that the effectiveness of CO_2 for the re-oxidation process of ceria was slow, *i.e.,* CO_2 was not a very effective oxidant in the re-oxidation of the oxygen defects. CO_2 started to breakthrough when the ceria surface was still largely reduced. NO

started, however, only to breakthrough when the surface was 75% re-oxidised. This CO_2 effectiveness behaviour could be either related to a slow desorption of CO or the negative driving force to the (*quasi-*) equilibrium between CO, CO_2, Ce^{3+}, and Ce^{4+}, according to Equation (3). The pulse of CO over a (pre-) oxidised ceria showed that CO could only reduce ceria up to 1 hypothetical ceria layer supported the existence of a (*quasi-*) equilibrium between CO, CO_2, Ce^{3+}, and Ce^{4+}. The inactivity of CO_2 could not be caused by the full coverage of CO on the ceria surface according the calculated carbon balance in Figure 3B.

Figure 4 (here)

In the Di-Air system, diesel fuel is used as reductant instead of CO and H_2. Therefore, the study on the performance of CO_2 over a fuel reduced ceria will be required. Propene was used to mimic diesel in the real practical operation. As displayed in **Figure 4**, phase I and phase II will be used to distinguish the full NO (CO_2) conversion (phase I) and NO (CO_2) started to breakthrough (phase II). The CO_2 conversion over C_3H_6 pre-reduced ceria is shown in Figure 4A and B. In contrast to the CO_2 conversion over a CO reduced ceria (**Figure 3A and B**), the CO_2 pulses over a C_3H_6 reduced ceria showed that CO_2 was completely converted till pulse number 6000 (phase I). CO was the only product. There was some more CO formation than was required for refilling the oxygen defects (Figure 4A). Apparently, some of the deposited carbon was converted from the catalyst as indicated from the carbon balance in Figure 4B. According to the oxygen balance in Equation 1, oxygen defects in the ceria were refilled during the CO_2 pulses. As shown in Figure 4B, when CO_2 started to breakthrough from pulse number 6000 onwards, oxygen refilling rate started to decline. The CO_2 conversion dropped from 100% in phase I to on average effectiveness of 20% in phase II. The quantity of oxygen refilling during phase I was around 50% of oxygen defects that was created by the C_3H_6 pre-treatment. The total sum of carbon consumption during the phase I and II was around 2% of deposited carbon formed during the C_3H_6 pre-treatment.

This full conversion time interval (phase I, **Figure 4A**) was due to the deeper degree of ceria reduction (2.8 hypothetical reduced ceria layers). The formation of carbonate by CO_2 pulse could be eliminated here since the carbon balance was negative, indicating that the CO_2 pulse will convert carbon deposits from the surface instead of carbon accumulation. The formation of CO during the CO_2 pulses will be a combination of both the CO_2 reduction and deposited carbon oxidation.

The majority of CO formation during phase I came from the reduction of CO_2 on the oxygen defects according to the carbon and oxygen balances in **Figure 4B** [20], as described by Equation 3. This observation confirmed the existence of a (*quasi-*) equilibrium between CO, CO_2, Ce^{3+}, and Ce^{4+}.

The oxidation of deposited carbon via lattice oxygen from ceria could be described [6, 26], according to equation 4:

$$C + 2Ce^{4+} + O^{2-} \rightarrow CO + 2Ce^{3+} \quad (4)$$

Therefore, the CO_2 pulses during phase I, where CO_2 was completely converted, led to an oxygen accumulation in the ceria, thus re-oxidising the oxygen defects.

CO_2 started to breakthrough from pulse number 6000 onwards, where 50% of oxygen defects were refilling and 2% of deposited carbon was oxidised (Figure 4B). CO_2 effectiveness started to drop when the ceria surface was still reduced.

One might argue that a gas-phase CO_2 could react with surface deposited carbon, forming CO directly according to Equation 5:

$$CO_2 + C \rightarrow 2CO \quad (5)$$

This reaction will be very unlikely since then for each converted CO_2 molecule two CO molecules should be generated, which was not supported by the observation in **Figure 4A**.

Figure 4C and **D** show the results of NO pulse over a C_3H_6 reduced ceria at 560 $^{\circ}$C. The pulse of NO resulted in the formation of N_2 and CO, followed by the formation of N_2 and CO_2. NO was completely converted during phase I and started to breakthrough from pulse number 30000 (phase II) onwards. The oxygen and carbon balances during the NO pulses are displayed in Figure 4D. The quantity of oxygen defect refilling during phase I was around 84%, which corresponded to around 60% of the surface layer of ceria was oxidised. The formation of CO and CO_2 during NO pulses indicated the conversion of deposited carbon from ceria surface. Total carbon conversion during phase I was around 90% of deposited carbon. Apparently, NO conversion only dropped when most of the deposited carbon was consumed.

Over C_3H_6 reduced ceria, NO showed full conversion till hardly any deposited carbon was left on the surface,, while CO_2 showed much lower CO_2 conversion rate than that of the NO, in the oxidation of the deposited carbon (Figure 4). As shown in Table 2, during the NO pulses, the consumption of deposited carbon increased from 8% to 90% from NO pulse number 5000 to 30000. During the CO_2 pulses, the consumption of deposited carbon only increased from 1.4% to 20%. Therefore, CO_2 was a less efficient oxidant in deposited carbon oxidation as compared to that of NO.

Table 2. Deposited carbon consumption by NO and CO_2 pulses over C_3H_6 reduced ceria in TAP.

		The number of gas pulses		
		5000	15000	30000
Deposited carbon consumption	CO_2	1.4%	8%	20%*
	NO	8%	42%	90%

* predicted data based on 20% CO_2 conversion

3.2.2. Investigation of CO_2 and NO reactivity over reduced ceria by *in-situ* Raman

Figure 5 (here)

In-situ Raman was applied to investigate the NO and CO_2 reactivities over reduced ceria under atmosphere pressure in a Linkam cell. The band at 460 cm^{-1} was attributed to the symmetric stretch mode of Ce-O_8 crystal unit (F_{2g} mode), which was characteristic for a oxidised fluorite ceria structure [27]. As shown in the **Figure 5A**, band at 460 cm^{-1} disappeared immediately with the C_3H_6 pre-treatment and this band intensity re-emerged and its intensity increased during CO_2 exposure, indicating that pre-reduced ceria was re-oxidised by CO_2. The bands at 1575 and 1350 cm^{-1} were assigned to G band and D band of carbon in either graphene or graphite form, respectively. The G band was usually assigned to zone centre phonons of E_{2g} symmetry of the perfect graphite structure, and the D peak was a breathing mode of A_{1g} symmetry. This mode was forbidden for a perfect

graphite structure and only became active in the presence of structural defects and disorders [28]. During the C_3H_6 pre-treatment, these two bands were formed only after the reduction of the ceria.. These two bands hardly changed in intensity upon CO_2 exposure (**Figure 5B**), indicating that CO_2 was only able to re-oxidise oxygen defects and not able to oxidise the carbon deposits.

Figure 6 (here)

In order to make a comparison between NO and CO_2 reactivity under atmosphere pressure, *in-situ* Raman spectroscopy was recorded during the NO flow over C_3H_6 reduced ceria at 560 $^{\circ}$C. In contrast to the CO_2 experiment, the band at 460 cm^{-1} significantly increased upon the NO exposure (**Figure 6A)**, indicating (re-)oxidation of oxygen defects by NO. Subsequently, after relilling the oxygen defects, the band at 1575 and 1350 cm^{-1} also started to significantly decrease (**Figure 6B),** indicating the oxidation of the deposited carbon.

3.2.3. Investigation of CO_2 and NO reactivity over reduced noble metal loaded ceria by TAP

The presence of noble metals on CeO_2 systems will promote the migration/exchange of oxygen species between isotopic $C^{18}O_2$ and $Pt/Ce^{16}O_2$ [10]. The presence of Pt accelerated the exchange rate between 200 and 400 $^{\circ}$C, mainly favouring the exchange of one of the oxygen atoms of $C^{18}O_2$ molecule [10]. The loading of noble metal over ceria might have an influence in either in assisting or inhibiting CO_2 reduction reactivity *versus* NO reactivity. Additionally, loadings of either Rh or Pd on ceria were able to promote the reduction of ceria surface and bulk to lower temperature by hydrogen, as evidenced by TPR, as indicated in **Figure 2**. However, the reduction of bare ceria required the temperatures exceeded 500 $^{\circ}$C for C_3H_6 and 540 $^{\circ}$C for C_3H_8 [19]. Here, to investigate the reactivity of CO_2 and NO towards the oxygen defects of noble metal loaded ceria, C_3H_6 was used as reductant to pre-treat the noble metal loaded ceria samples. Table 3 summarises the result of C_3H_6 pre-treatment over Rh/ceria and Pd/ceria at 450 $^{\circ}$C.

Table 3. Summary of oxygen defects and deposited carbon by C_3H_6 pre-treatment over Rh/ceria and Pd/ceria.

	T/ °C	Oxygen defects		Deposited carbon (carbon atoms/ mg_{cat})
		Oxygen atoms/ mg_{cat}	Ceria reduction layers	
Rh/ceria	450	$8.2 \cdot 10^{17}$	3	$8.7 \cdot 10^{17}$
Pd/ceria	450	$7.3 \cdot 10^{17}$	2.8	$4.4 \cdot 10^{17}$

Figure 7 (here)

The results of CO_2 pulses over C_3H_6 reduced Rh/ceria are shown in **Figure 7A and B**. CO_2 was completely converted during phase I (pulse number 0-2000, **Figure 7A**), more CO was formed than the quantity of pulsed CO_2 molecules was dosed. CO_2 started to breakthrough after pulse number 2000. According to Equation 1 and 2, the oxygen balance and carbon balance were plotted, as shown in Figure 7B. The oxygen balance showed that the quantity of oxygen accumulation during phase I was around 40% of oxygen defects that created by the C_3H_6 pre-treatment. The oxygen accumulation dropped at the same point when the CO_2 effectiveness started to decline, when the ceria surface was still reduced. The carbon balance indicated that around 2% of deposited carbon was oxidised. Initially the oxygen from the pulsed CO_2 was used to refill the oxygen defects and those re-oxidised ceria defects were immediately partially used for the oxidation of the deposited carbon. After this initial phase the CO_2 effectiveness dropped when still a large amount of deposited carbon on the Rh/ceria sample was present. The re-oxidation rate of the remaining oxygen defects was inhibited at the same time.

Similarly to the experiment over Rh/ceria, the experiment of CO_2 pulses over C_3H_6 reduced Pd/ceria at 450 °C was performed (**Figure 7C and D**). The CO_2 conversion was complete during phase I (0-1200

pulse number) and its conversion dropped during phase II. The oxygen and carbon balances (Figure 7D) indicated around of 30% of the oxygen defects had been refilled and only 1% of the deposited carbon was converted during phase I. CO_2 conversion started to drop when the surface of ceria was still reduced. In phase II the remaining deposited carbon hindered the re-oxidation of the oxygen defects and subsequently also the conversion rate of the deposited carbon.

Figure 8 (here)

As compared to the results of CO_2 over C_3H_6 reduced ceria, the loading of noble metals, both Rh and Pd, did not change the reactivity of CO_2 in oxidising the deposited carbon. The deposited carbon consumptions during the full CO_2 conversion (phase I) for Rh and Pd loaded ceria were only 2% and 1%, respectively. CO_2 was mainly used to refill the oxygen vacancies of ceria, regardless of the presence of noble metal. CO_2 conversion started to drop when the surface of ceria was still almost completely reduced.

In order to make a comparison between CO_2 and NO reactivity over the noble metal loaded ceria, NO pulse experiments were performed over Rh/ceria and Pd/ceria with the same degree of ceria reduction and amount of deposited carbon.

The pulse of NO over a C_3H_6 reduced Rh/Ceria at 450 $^{\circ}$C showed that NO showed full conversion at a time interval of 12000 pulses (phase I, **Figure 8A**), followed by NO effectiveness dropped to zero during phase II. The oxygen balance indicated the oxygen defects in the Rh/ceria sample during phase I that approximately 80% of oxygen defects were refilled. At the same time the carbon balance indicated that 90% of the total deposited carbon was oxidised to either CO or CO_2 (**Figure 8A**).

Similarly to Rh/ceria, the NO pulse experiment over the C_3H_6 reduced Pd/Ceria at 450 $^{\circ}$C showed that NO showed full conversion for 7000 pulses (phase I, **Figure 8B**). During phase I, around 90% of oxygen defects were refilled and around 70% of deposited carbon was oxidised. To obtain the same degree of ceria re-oxidation and deposited carbon consumption, more NO pulses were needed for Rh/ceria than that for Pd/ceria due to the fact that the amount of deposited carbon on Rh/ceria was 2 times of that on Pd/ceria (Table 3).

Even in the presence of noble metals, the pulses of NO still mainly led to the oxygen accumulation into ceria lattice, followed by the oxidation of deposited carbon.. NO conversion started to drop when 70% of the ceria surface was re-oxidised. In general, the loading of noble metal did not influence the reactivity of NO. As shown in **Table 4**, the pulses of NO and CO_2 led to 2% and 5% deposited carbon consumption during the first 2000 pulses, respectively. However, the deposited carbon consumption raised to 55% when 8000 pulses of NO were introduced while it was 16% after 8000 CO_2 pulses. This difference in deposited carbon consumption was further observed with pulse number. For 12000 pulses, the pulse of NO led to 90% deposited consumption while only 20% for CO_2 pulses. Based on the above results for CO_2 and NO pulse experiments, NO was a much more efficient oxidant in oxidising deposited carbon than CO_2, even in the presence of noble metal.

Table 4. Deposited carbon consumption by NO and CO_2 pulses over C_3H_6 reduced Rh/ceria at 450 ^oC in TAP.

		The number of gas pulses		
		2000	8000	12000
Deposited carbon consumption	CO_2	2%	16%	20%
	NO	5%	55%	90%

3.2.4. Investigation of CO_2 and NO reactivity over reduced Rh/ceria support by flow reactor

Similarly to TAP experiments, 1.25% C_3H_6 in helium was used as the reductant to pre-treat the Rh/ceria for 2 h in the flow reactor at 450 ^oC. The pre-treatment of C_3H_6 led to $8.2 \cdot 10^{17}$ carbon atoms/mg_{cat} deposition and around 3 layers of ceria reduction.

Figure 9 showed the results upon the exposure of 0.2% NO in He over C_3H_6 reduced Rh/ceria at 450 ^oC with GHSV of 67.000 L/L/h. Figure 9A and B shows the MS and FT-IR response of gasses at the exit of the reactor. m/e = 28 was observed, which was attributed to the formation of N_2 and CO. The formation of CO was confirmed by the FT-IR (Figure 9B). NO was not detected by FT-IR during the first 450 s, followed by a gradual signal increment in both MS and IR response. Low intensity of m/e

=44 was observed, which was attributed to the formation of CO_2. FT-IR results also confirmed the formation of CO_2 and excluded the formation of N_2O during the whole NO gas stream exposure, , as shown in Figure 9B. NO_2 formation was not observed before 2000 s and less than 10 ppm of NO_2 was observed in FT-IR after 2000 s. Therefore, over the reduced ceria surface, NO was reduced into N_2. Several ppm of NO was oxidised into NO_2 over oxidised ceria surface promoted by Rh. The formation of only $^{15}N_2$ during the NO reduction was also foundby using ^{15}NO, as reported in our previous work [7]. The reduced ceria was fully re-oxidised and the total quantity of CO and CO_2 formed during the NO exposure was calculated to be $8 \cdot 10^{17}$, which was almost equal to the carbon deposition by C_3H_6 pre-treatment.

Figure 9 (here)

Figure 10 (here)

Figure 10 shows the results of the exposure of 0.2% CO_2 in He over the C_3H_6 reduced Rh/ceria at 450 ^oC with GHSV of 67.000 L/L/h. m/e=28 and m/e=44 were observed in the MS response (Figure 10A), attributed to the CO and CO_2, respectively. CO_2 immediately broke through during the CO_2 exposure. The FT-IR was also used to further quantify CO and CO_2 at the exit of reactor (Figure 10B). The reduced ceria was fully re-oxidised and the amount of carbon consumption was calculated to be $8.2 \cdot 10^{16}$ carbon atoms/mg_{cat}, which was around 10% of the total deposited carbon. The result of Figure 10 confirmed that from TAP experiments, *i.e.,* CO_2 was a mild oxidant and the deposited carbon can hardly oxidised during the CO_2 exposure.

Figure 11 (here)

In order to support our observation of firstly the re-oxidation of the ceria for Rh/ceria catalyst and subsequently the oxidation of the deposited carbon an additional Raman experiment was carried for a hydrocarbon reduced Rh/ceria upon NO exposure. The on-line Raman probe detected the changes of the Rh/ceria surface spectroscopy during the NO gas stream (**Figure 11**), performed at 500 ^oC. During the NO gas stream, the band at 460 cm^{-1} emerged and its intensity increased (**Figure 11A**), subsequently the intensities of the “carbon” bands at 1350 and 1575 cm^{-1} completely disappeared (**Figure 11B**). The increase of band at 460 cm^{-1} indicated the re-oxidation of reduced ceria and the

disappearance of bands at 1350 and 1575 cm^{-1} demonstrated the completely conversion of the deposited carbon upon NO exposure. The results of NO reduction in the flow reactor in **Figure 9** and **Figure 11** were consistent with the results from TAP results. NO can be selectively reduced into N_2 and the deposited carbon can be oxidised during the NO exposure.

For a typical diesel exhaust composition, approximately several hundred ppm NO had to compete with an excess of 5% O_2, 5% CO_2, and 5-10% H_2O in order to meet the future automotive legislation emission standards. Although the results from TAP experiment showed that NO was able to be reduced into N_2 on oxygen defect sites, it was still a question whether NO was able to reduce into N_2 in the presence of excess CO_2. Therefore, 0.2% of NO was used to compete with 5% CO_2 over C_3H_6 reduced Rh/ceria at 450 $^{\circ}C$. As shown in **Figure 12A**, NO started to breakthrough after 410 s. m/e = 28 was observed, related to the formation of N_2 and CO. m/e = 44 immediately broke through during the CO_2 exposure and stable around 5%. There was no N_2O and NO_2 formation as confirmed by FT-IR (**Figure 12B**). Both N_2 and CO were observed without detection of any N_2O and NO_2 (detection limit 1ppm), indicating that NO was completely selectively reduced into N_2 in CO_2 excess. The total quantities of converted NO and CO_2 were calculated to be $1.1 \cdot 10^{18}$ NO molecules/mg_{cat} and $5 \cdot 10^{17}$ CO_2 molecules/mg_{cat}, respectively. Although the CO_2 concentration was 25 times larger than that of NO, the number of converted NO molecules was around 2.2 times higher than that of converted CO_2. More importantly, the reduction of CO_2 mainly occurred during the first 80 s, and CO_2 was hardly reactive during time from 80 s to 410 s, where still full NO conversion was observed. The carbon balance of **Figure 12B** was plotted in **Figure 12C**. The amount of carbon consumption during the first 80 s was calculated to be $8.8 \cdot 10^{16}$, which was around 10% of total deposited carbon. Therefore, the majority of deposited carbon was consumed by NO reduction into N_2. The reduction of CO_2 into CO occurred mainly over the reduced sites of ceria, refilling the oxygen defects. Once the oxygen defects were refilled the CO_2 effectiveness completely vanished.

Figure 12 (here)

3.3. CO_2 *versus* NO reactivity evaluation

Although CO_2 was able to oxidise the oxygen defects on the CO pre-reduced ceria, but the effectiveness of the CO_2 re-oxidation was low since the CO_2 conversion dramatically declined after only a few CO_2 pulses as shown in **Figure 3A** and **B**. Up to 2000 CO_2 pulses, only 50% of oxygen defects were refilled. Regarding the C_3H_6 pre-reduced ceria, it can be concluded that the CO_2 to some extent, was used for the re-oxidation of oxygen defects. CO_2 pulses will hardly consume any deposited carbon (**Figure 4A and B**). The *in-situ* Raman experiments under atmosphere pressure (Figure 6A and B) also pointed out that CO_2 was a mild oxidant in oxidising the reduced ceria and it can hardly oxidise the deposited carbon. Even with noble metal loading, both the TAP pulse experiment (Figure 7) and the flow reator (Figure 10) under atmoshphere indicated that CO_2 can l hardly oxidise the deposited carbon.

In contrast, NO pulses over C_3H_6 reduced ceria sample showed NO was completely reduced into N_2 (phase I, Figure 4C), where 84% of oxygen defects were refilled and 90% of the deposited carbon was oxidised (Figure 4D). The TAP pulses experiments confirmed that NO was more efficient oxidant for refilling oxygen defects and oxidation of deposited carbon, as compared to CO_2. The flow reactor experiments under atmosphere further confirmed that the NO can be reduced into N_2 and oxidise the deposited carbon. The *in-situ* Raman experiments supported the same TAP and flow experimental observations that NO can re-oxidise the reduced ceria and oxidise deposited carbon.

CO_2 and NO competition experiment over the C_3H_6 pre-reduced Rh/ceria in flow reactor indicated that NO is more powerful reductants in competing for the oxygen defects (**Figure 12**). Around 90% of deposited carbon was consumed by NO. NO was selectively reduced into N_2 regardless of CO_2 presence.

In the Di-Air system, total oxygen defects capacity, including the oxygen defects of ceria and the deposited carbon, determined the quantity of NO molecules that can be converted into N_2. Fuel injection is used to create the oxygen defect capacity and carbon deposits. The low reactivity of CO_2 towards oxygen defects and deposited carbon over both reduce ceria and noble metal reduced ceria implies that the most of the fuel will be used for reduction NO into N_2 and not the conversion of CO_2.

4. Conclusions

1. CO_2 is a mild oxidant in the oxidation of oxygen defects of ceria due to the existence of a (*quasi*-) equilibrium between CO, CO_2, Ce^{3+}, and Ce^{4+}. The deposited carbon, generated during C_3H_6 (fuel) pre-treatment, will hardly convert during CO_2 exposure.

2. The loading of noble metals, *e.g.,* Rh and Pd, on the ceria hardly changed the reactivity of CO_2 in the oxidation of oxygen defects and deposited carbon.

3. Compared to CO_2, NO was a much stronger oxidant. The deposited carbon can be oxidised during the NO exposure.

4. Traces of NO were able to compete with an excess of CO_2 for oxygen vacancies over Rh/ceria. The presence of CO_2 in the exhaust gas streams of lean burn engines will not significantly affect the NO reduction efficiency.

Acknowledgements

The authors wish to acknowledge financial support by the China Scholarship Council (CSC).

References

[1] Y. Ikeda, K. Sobue, S. Tsuji, S.i. Matsumoto, Development of NO_x Storage-Reduction Three-way Catalyst for D-4 Engines, SAE Technical Paper 1999-01-1279, 1999.
[2] W.R. Miller, J.T. Klein, R. Mueller, W. Doelling, J. Zuerbig, The Development of Urea-SCR Technology for US Heavy Duty Trucks, SAE Technical Paper 2000-01-0190, 2000.
[3] F. Can, X. Courtois, S. Royer, G. Blanchard, S. Rousseau, D. Duprez, An overview of the production and use of ammonia in NSR + SCR coupled system for NO_x reduction from lean exhaust gas, Catal Today., 197 (2012) 144-154.
[4] Y. Bisaiji, K. Yoshida, M. Inoue, K. Umemoto, T. Fukuma, Development of Di-Air-A New Diesel deNOx System by Adsorbed Intermediate Reductants, SAE International Journal of Fuels and Lubricants, SAE Techical Paper 2012-01-1744, 5 (2012) 380-388.
[5] M. Inoue, Y. Bisaiji, K. Yoshida, N. Takagi, T. Fukuma, $DeNO_x$ Performance and Reaction Mechanism of the Di-Air System, Top. Catal., 56 (2013) 3-6.
[6] Y. Wang, J. Posthuma de Boer, F. Kapteijn, M. Makkee, Next Generation Automotive $DeNO_x$ Catalysts: Ceria What Else?, ChemCatChem, 8 (2016) 102-105.
[7] , Y. Wang, R. Oord, D. van der Berg, B.M. Weckhuysen, M. Makkee, Oxygen Vacancies in reduced Rh-and Pt-ceria for Highly Selective and Reactive Reduction of NO into N_2 in excess of O_2, ChemCatChem, 9 (2017) 2935-2939.
[8] S. Sharma, S. Hilaire, J. Vohs, R. Gorte, H.-W. Jen, Evidence for oxidation of ceria by CO_2, J. Catal., 190 (2000) 199-204.
[9] W.C. Chueh, C. Falter, M. Abbott, D. Scipio, P. Furler, S.M. Haile, A. Steinfeld, High-flux solar-driven thermochemical dissociation of CO_2 and H_2O using nonstoichiometric ceria, Science, 330 (2010) 1797-1801.
[10] A. Bueno-López, K. Krishna, M. Makkee, Oxygen exchange mechanism between isotopic CO_2 and Pt/CeO_2, Appl. Catal. A., 342 (2008) 144-149.
[11] O. Demoulin, M. Navez, J.-L. Mugabo, P. Ruiz, The oxidizing role of CO_2 at mild temperature on ceria-based catalysts, Appl. Catal. B., 70 (2007) 284-293.
[12] M. Bradford, M. Vannice, CO_2 reforming of CH_4, Catal. Rev., 41 (1999) 1-42.
[13] L.G. Appel, J.G. Eon, M. Schmal, The CO_2-CeO_2 interaction and its role in the CeO_2 reactivity, Catal. Lett., 56 (1998) 199-202.
[14] L. Katta, P. Sudarsanam, G. Thrimurthulu, B.M. Reddy, Doped nanosized ceria solid solutions for low temperature soot oxidation: Zirconium versus lanthanum promoters, Appl. Catal. B, 101 (2010) 101-108.
[15] V. Perrichon, A. Laachir, S. Abouarnadasse, O. Touret, G. Blanchard, Thermal stability of a high surface area ceria under reducing atmosphere, Appl. Catal. A., 129 (1995) 69-82.
[16] Y. Wang, J.P. de Boer, F. Kapteijn, M. Makkee, Fundamental Understanding of the Di-Air System: The Role of Ceria in NO_x Abatement, Top. Catal., (2016) 1-7.
[17] H.C. Yao, Y.F.Y. Yao, Ceria in automotive exhaust catalysts: I. Oxygen storage, J. Catal., 86 (1984) 254-265.
[18] H. Zhu, Z. Qin, W. Shan, W. Shen, J. Wang, Pd/CeO_2–TiO_2 catalyst for CO oxidation at low temperature: a TPR study with H_2 and CO as reducing agents, J. Catal., 225 (2004) 267-277.
[19] Y. Wang, M. Makkee, Fundamental understanding of the Di-Air system (an alternative NOx abatement technology). I: The difference in reductant pre-treatment of ceria, Appl. Catal. B, (2017) accepted (DOI: 10.1016/j.apcatb.2017.04.054).
[20] T. Staudt, Y. Lykhach, N. Tsud, T. Skala, K. Prince, V. Matolín, J. Libuda, Ceria reoxidation by CO_2: a model study, J. Catal., 275 (2010) 181-185.
[21] K. Chen, A.T. Bell, E. Iglesia, The relationship between the electronic and redox properties of dispersed metal oxides and their turnover rates in oxidative dehydrogenation reactions, J. Catal., 209 (2002) 35-42.
[22] G.N. Vayssilov, M. Mihaylov, P.S. Petkov, K.I. Hadjiivanov, K.M. Neyman, Reassignment of the vibrational spectra of carbonates, formates, and related surface species on ceria: a combined density functional and infrared spectroscopy investigation, J. Phys. Chem. C., 115 (2011) 23435-23454.
[23] C. Binet, M. Daturi, J.-C. Lavalley, IR study of polycrystalline ceria properties in oxidised and reduced states, Catal Today., 50 (1999) 207-225.
[24] Z. Cheng, B.J. Sherman, C.S. Lo, Carbon dioxide activation and dissociation on ceria (110): A density functional theory study, J. Chem. Phys., 138 (2013) 014702.
[25] R. Compton, P. Reinhardt, C. Cooper, Collisional ionization of Na, K, and Cs by CO_2, COS, and CS2: Molecular electron affinities, J. Chem. Phys., 63 (1975) 3821-3827.

[26] A. Bueno-Lopez, K. Krishna, M. Makkee, J.A. Moulijn, Active oxygen from CeO_2 and its role in catalysed soot oxidation, Catal. Lett., 99 (2005) 203-205.
[27] W. Weber, K. Hass, J. McBride, Raman study of CeO_2: second-order scattering, lattice dynamics, and particle-size effects, Phys. Rev. B., 48 (1993) 178.
[28] A.C. Ferrari, J. Robertson, Interpretation of Raman spectra of disordered and amorphous carbon, Phys. Rev. B., 61 (2000) 14095.

Captions

Figure 1. XRD pattern of ceria, Rh/ceria, and Pd/ceria.

Figure 2. H_2-TPR profiles of ceria, Rh/ceria, and Pd/ceria.

Figure 3. CO_2 pulse responses in TAP at 580 $^{\circ}$C (A and B) and NO pulse responses at 540 $^{\circ}$C (C and D) over 580 $^{\circ}$C and 540 $^{\circ}$C CO reduced ceria, respectively.

Figure 4. CO_2 pulse response in TAP at 580 $^{\circ}$C(A and B) and NO pulses at 560 °C (C and D) over C_3H_6 reduced ceria at 580 and 560 $^{\circ}$C, respectively.

Figure 5. *In-situ* Raman of CO_2 exposure over C_3H_6 reduced ceria at 560 $^{\circ}$C: (A) Ce-O_8 band of ceria at 460 cm^{-1} and (B) D band and G band of carbon at 1350 and 1575 cm^{-1}, respectively.

Figure 6. *In-situ* Raman of NO exposure over C_3H_6 reduced ceria at 560 $^{\circ}$C: (A) Ce-O_8 band of ceria at 460 cm^{-1} and (B) D band and G band of carbon at 1350 and 1575 cm^{-1}, respectively.

Figure 7. CO_2 pulse over at 450 $^{\circ}$C C_3H_6 reduced Rh/ceria (A and B) and Pd/ceria (C and D). (A) and (C) gas evolution during the CO_2 pulses, and (B) and (D) oxygen and carbon balances.

Figure 8. Oxygen and carbon balance, and NO conversion *versus* pulse number during NO pulse over at 450 $^{\circ}$C C_3H_6 reduced Rh/ceria (A) and Pd/ceria (B).

Figure 9. Reduction of NO over C_3H_6 pre-reduced Rh/ceria in a flow reactor at 450 ^{o}C; (A) MS and (B) FT-IR analysis.**Figure 10**. Reduction of CO_2 over C_3H_6 pre-reduced Rh/ceria in a flow reactor at 450 ^{o}C; (A) MS and (B) FT-IR analysis.

Figure 11. *In-situ* Raman of NO exposure over C_3H_6 reduced Rh/ceria at 500 $^{\circ}$C: (A) Ce-O_8 band at 460 cm^{-1} and (B) D band and G band at 1350 and 1575 cm^{-1}, respectively.

Figure 12. Reduction of NO in the presence of excess CO_2 over C_3H_6 pre-reduced Rh/ceria in a flow reactor at 450 ^{o}C; (A) MS analysis, (B) and (C) FT-IR analysis.

.

Table 1. Summary of oxygen defects and deposited carbon by CO and C_3H_6 pre-treatment over ceria.

	T/ °C	Oxygen defects		Deposited carbon (carbon atoms/ mg_{cat})
		Oxygen atoms/ mg_{cat}	Ceria reduction layers	
CO	580	$3 \cdot 10^{17}$	1	-
	540	$3 \cdot 10^{17}$	1	-
C_3H_6	580	$7.1 \cdot 10^{17}$	2.8	$1.5 \cdot 10^{18}$
	560	$5.9 \cdot 10^{17}$	2.3	$1 \cdot 10^{18}$

Table 2 Deposited carbon consumption by NO and CO_2 pulses over C_3H_6 reduced ceria in TAP.

		The number of gas pulses		
		5000	15000	30000
Deposited carbon consumption	CO_2	1.4%	8%	20%
	NO	8%	42%	90%

Table 3. Summary of oxygen defects and deposited carbon by C_3H_6 pre-treatment over Rh/ceria and Pd/ceria.

	T/ °C	Oxygen defects		Deposited carbon (carbon atoms/ mg_{cat})
		Oxygen atoms/ mg_{cat}	Ceria reduction layers	
Rh/ceria	450	$8.2 \cdot 10^{17}$	3	$8.7 \cdot 10^{17}$
Pd/ceria	450	$7.3 \cdot 10^{17}$	2.8	$4.4 \cdot 10^{17}$

Table 4. Deposited carbon consumption by NO and CO_2 pulses over C_3H_6 reduced Rh/ceria at 450 °C in TAP.

		The number of gas pulses		
		2000	8000	12000
Deposited carbon consumption	CO_2	2%	16%	20%
	NO	5%	55%	90%

Figures

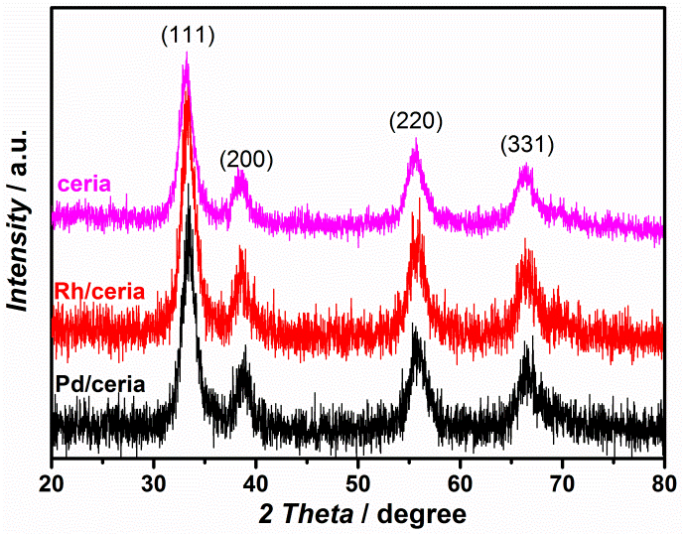

Figure 1. XRD pattern of ceria, Rh/ceria, and Pd/ceria.

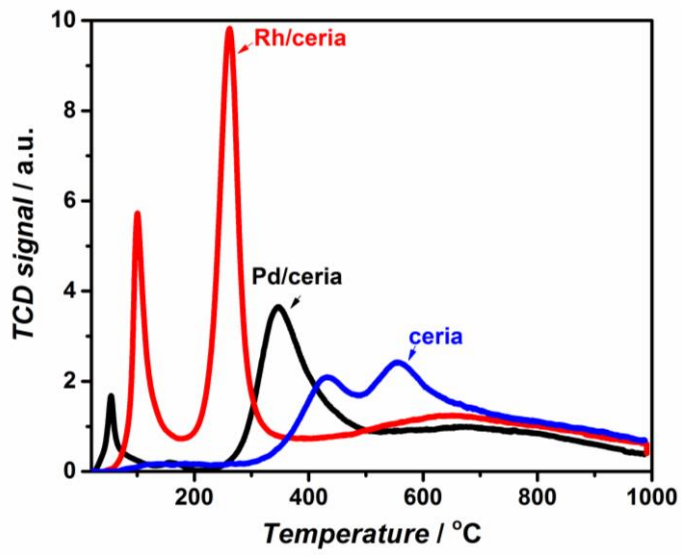

Figure 2. H_2-TPR profiles of ceria, Rh/ceria, and Pd/ceria.

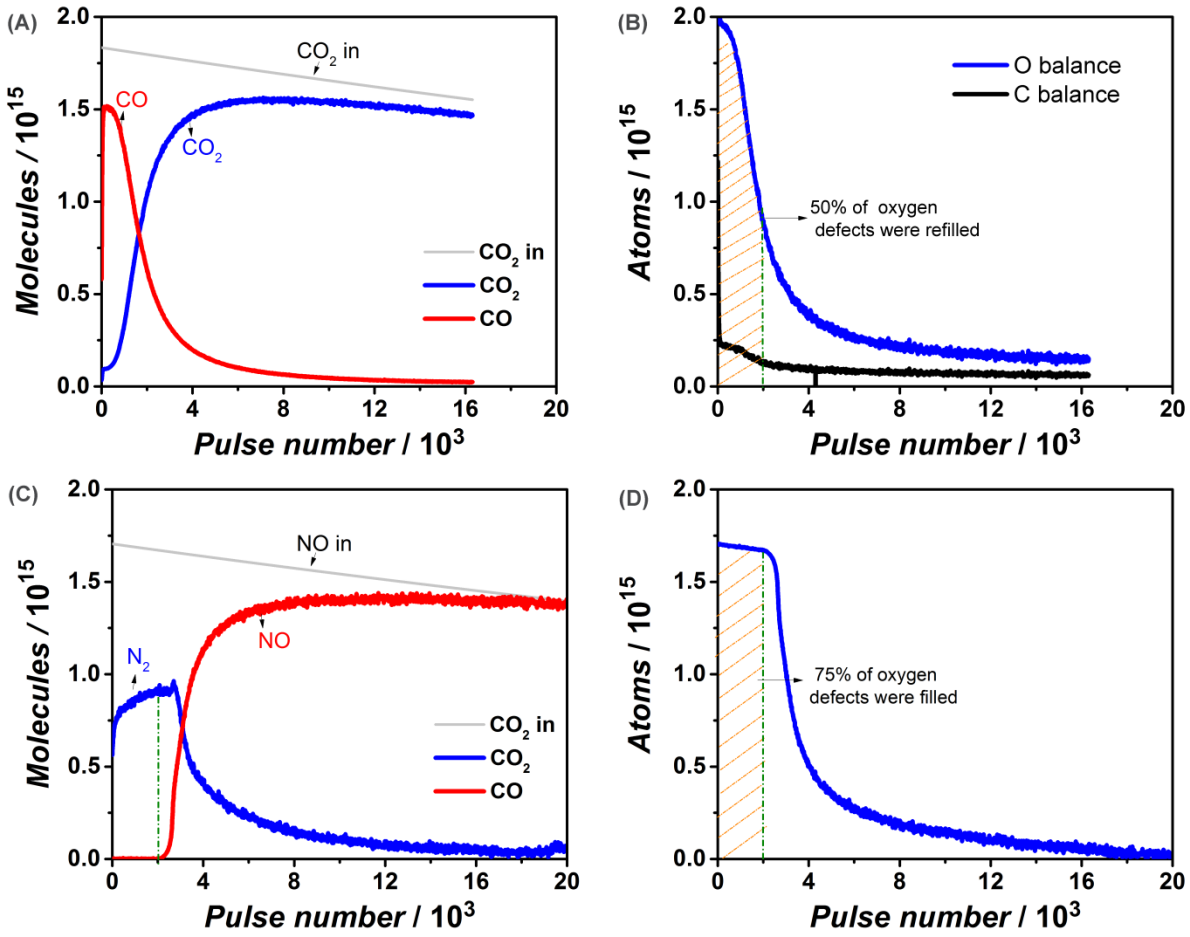

Figure 3. CO_2 pulse responses in TAP at 580 °C (A and B) and NO pulse responses at 540 °C (C and D) over CO reduced ceria at 580 °C and 540 °C, respectively.

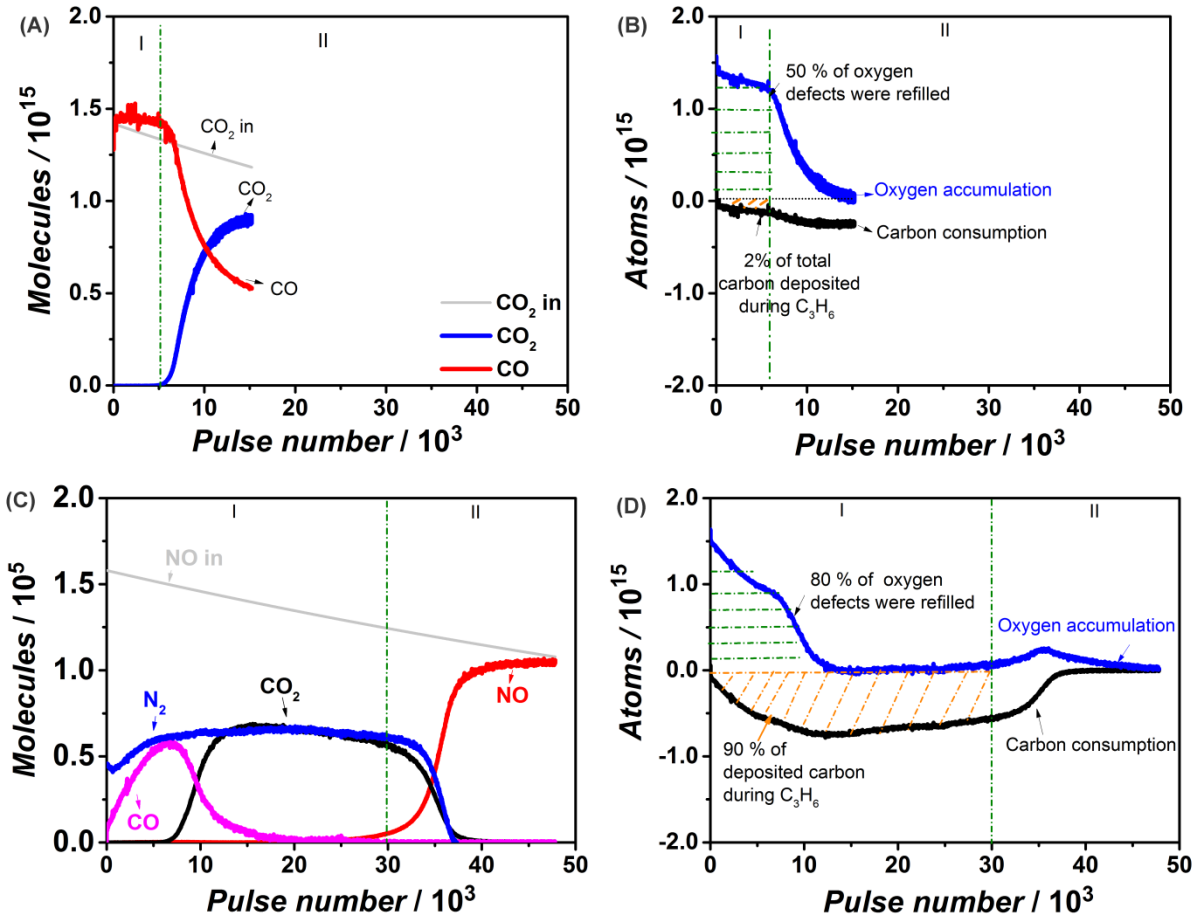

Figure 4. CO_2 pulse response in TAP at 580 °C(A and B) and NO pulses at 560 °C (C and D) over C_3H_6 reduced ceria at 580 and 560 °C, respectively.

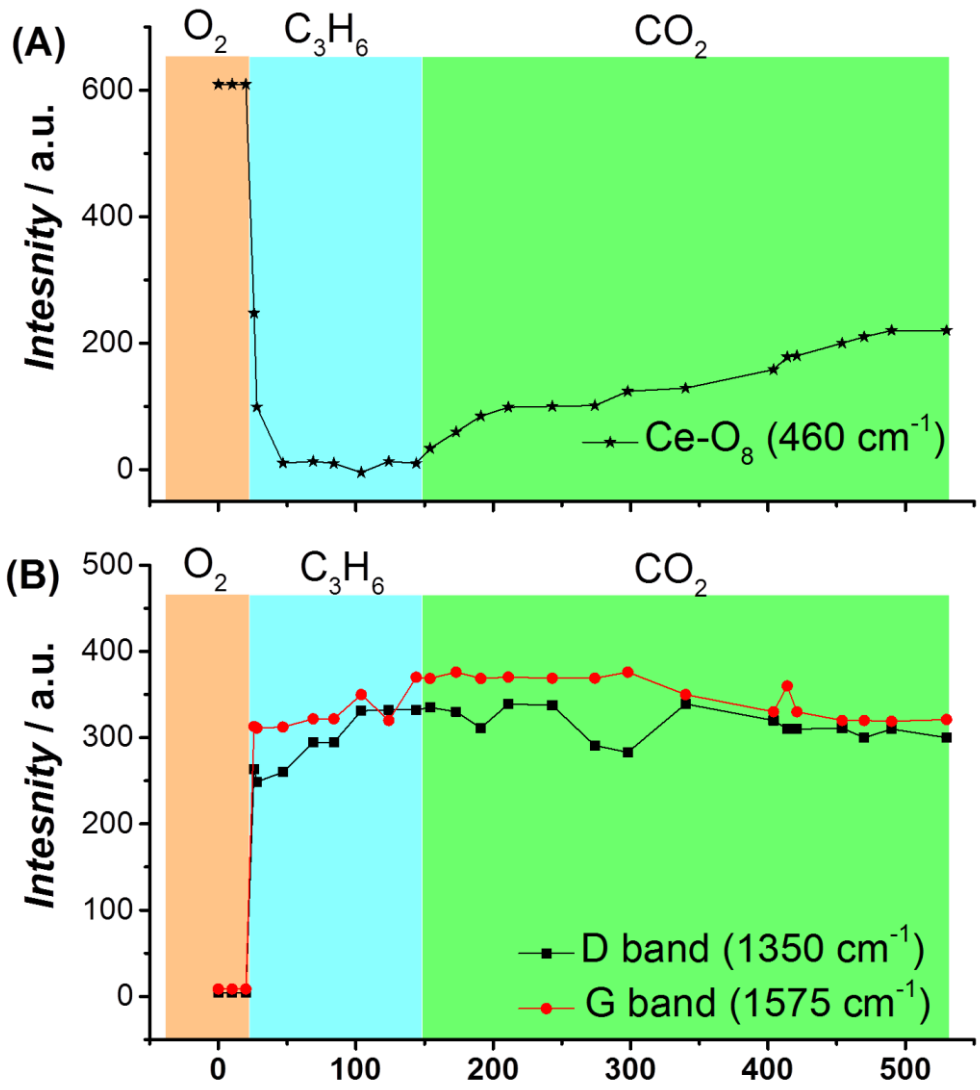

Figure 5. *In-situ* Raman of CO_2 exposure over C_3H_6 reduced ceria at 560 °C: (A) Ce-O_8 band of ceria at 460 cm^{-1} and (B) D band and G band of carbon at 1350 and 1575 cm^{-1}, respectively.

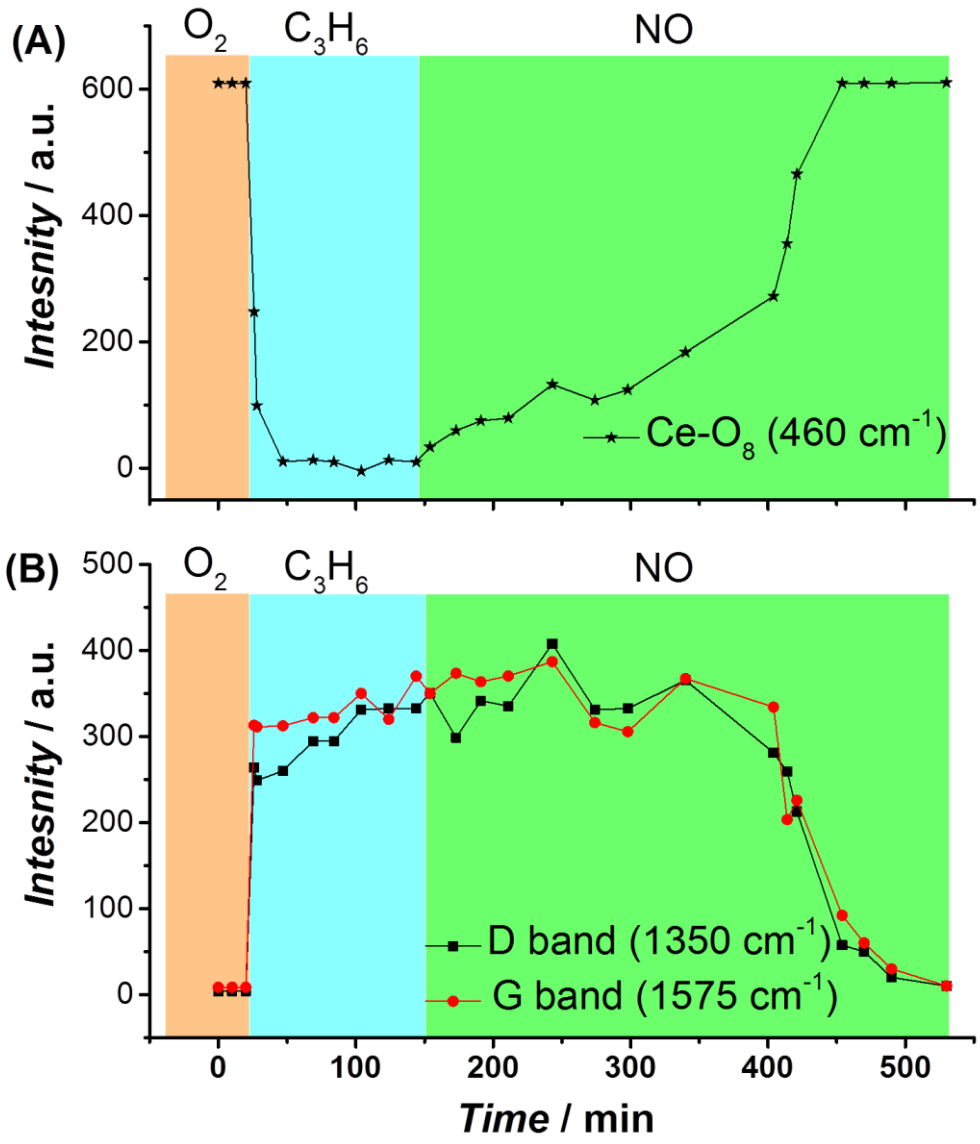

Figure 6. *In-situ* Raman of NO exposure over C_3H_6 reduced ceria at 560 °C: (A) Ce-O_8 band of ceria at 460 cm^{-1} and (B) D band and G band of carbon at 1350 and 1575 cm^{-1}, respectively.

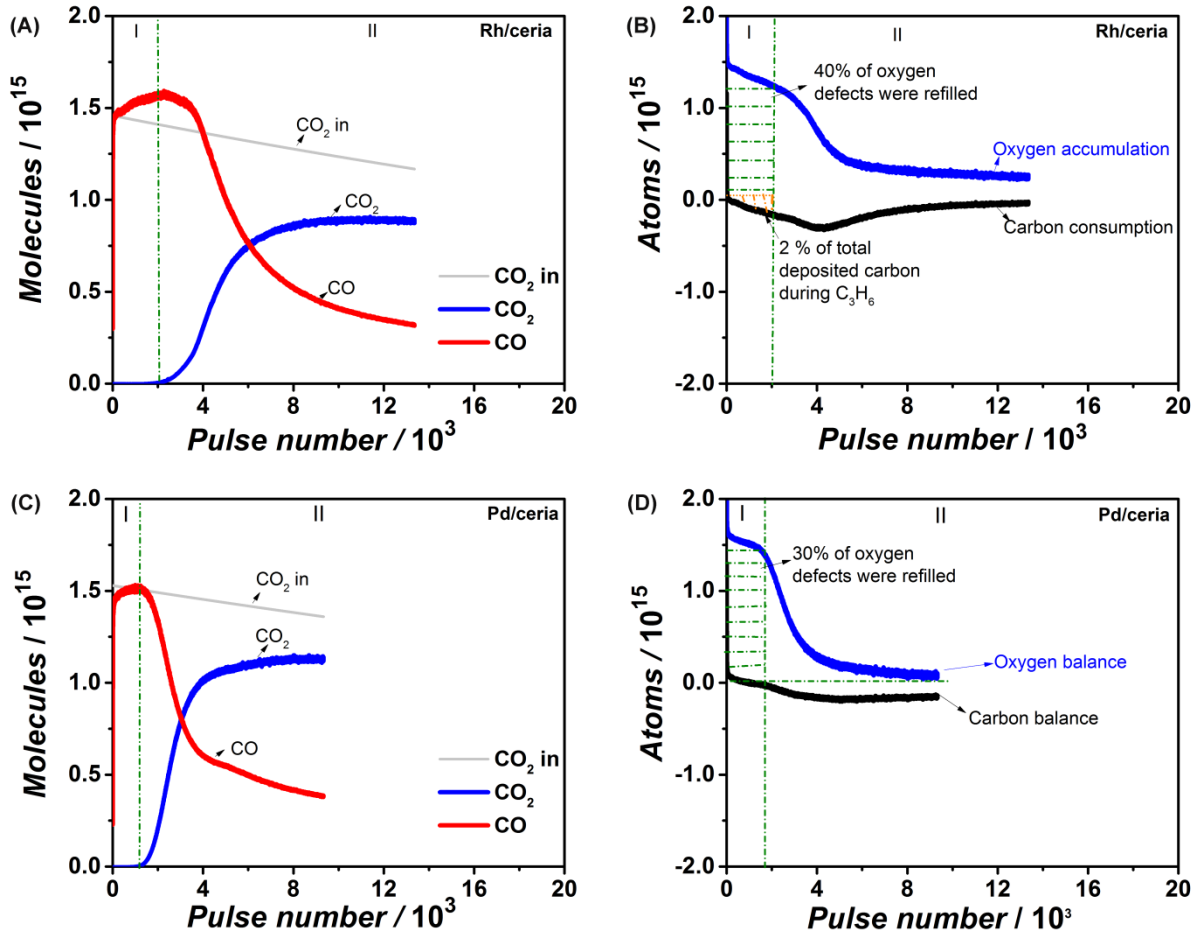

Figure 7. CO_2 pulse over at 450 °C C_3H_6 reduced Rh/ceria (A and B) and Pd/ceria (C and D). (A) and (C) gas evolution during the CO_2 pulses, and (B) and (D) oxygen and carbon balances.

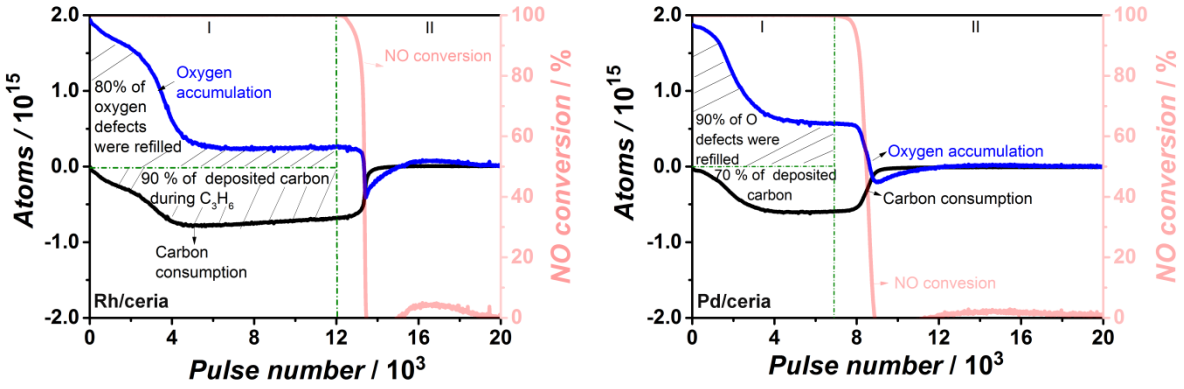

Figure 8. Oxygen and carbon balance, and NO conversion *versus* pulse number during NO pulse at 450 °C over C_3H_6 reduced Rh/ceria (A) and Pd/ceria (B).

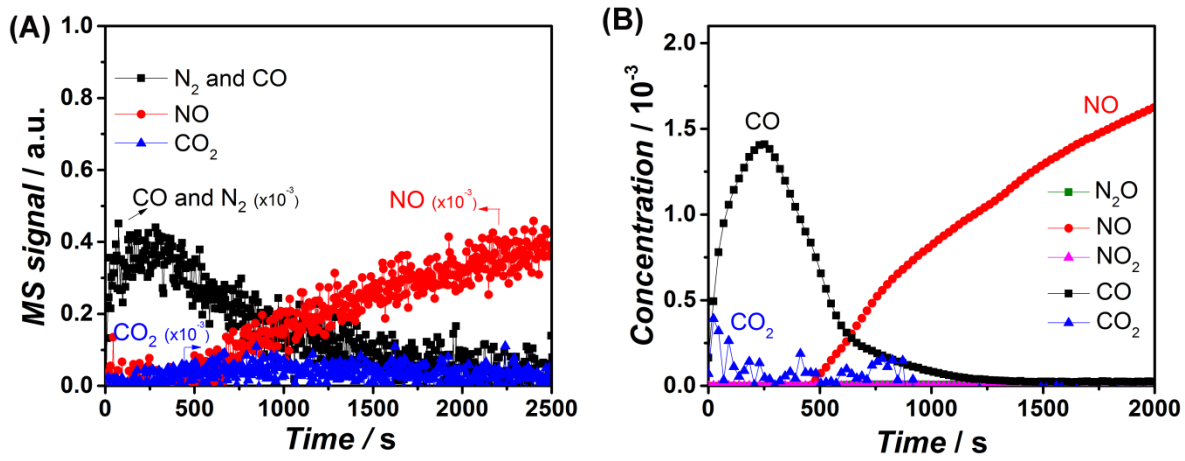

Figure 9. Reduction of NO over C_3H_6 pre-reduced Rh/ceria in a flow reactor at 450 ^oC; (A) MS and (B) FT-IR analysis.

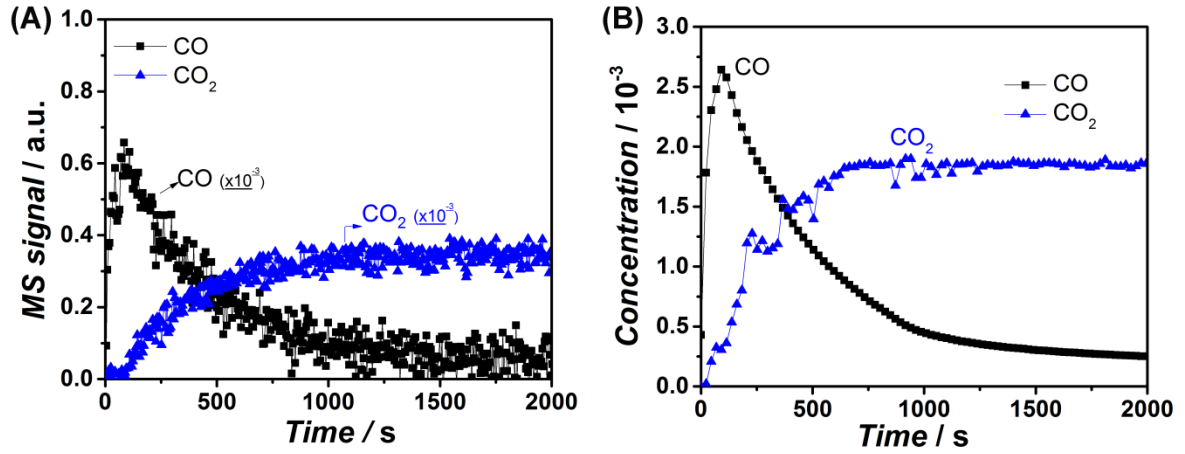

Figure 10. Reduction of CO_2 over C_3H_6 pre-reduced Rh/ceria in a flow reactor at 450 ^oC; (A) MS and (B) FT-IR analysis.

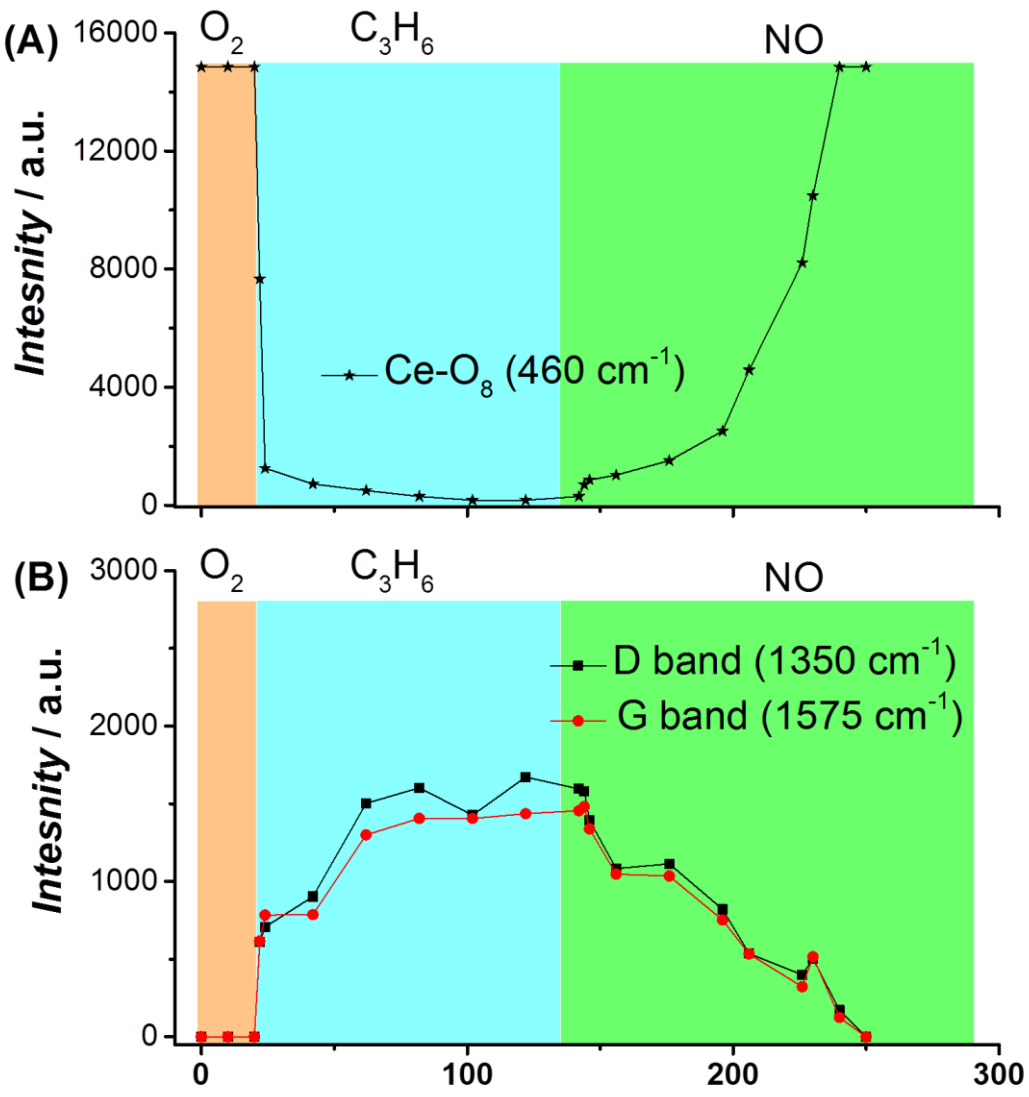

Figure 11. *In-situ* Raman of NO exposure over C_3H_6 reduced Rh/ ceria at 500 °C: (A) Ce-O_8 band of ceria at 460 cm^{-1} and (B) D band and G band of carbon at 1350 and 1575 cm^{-1}, respectively

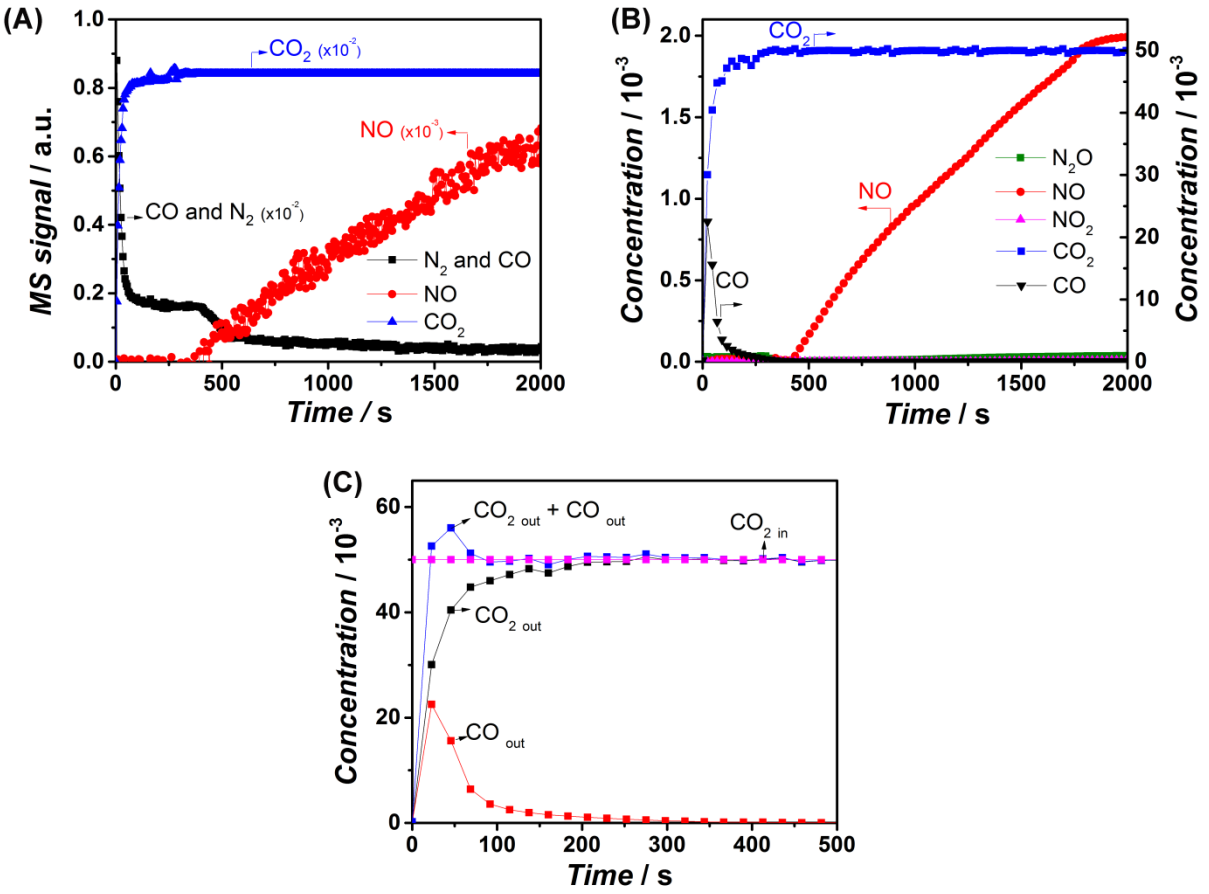

Figure 12. Reduction of NO in the presence of excess CO_2 over C_3H_6 pre-reduced Rh/ceria in a flow reactor at 450 ^{o}C; (A) MS analysis, (B) and (C) FT-IR analysis.